

# Self-Supervised Object-in-Gripper Segmentation from Robotic Motions

Wout Boerdijk<sup>1</sup>, Martin Sundermeyer<sup>1</sup>, Maximilian Durner<sup>1</sup> and Rudolph Triebel<sup>1,2</sup>

<sup>1</sup>German Aerospace Center (DLR)

82234 Wessling, Germany

<sup>2</sup>Technical University of Munich (TUM)

80333 Munich, Germany

E-mail: {wout.boerdijk, martin.sundermeyer, maximilian.durner, rudolph.triebel}@dlr.de

**Abstract**—We present a novel technique to automatically generate annotated data for important robotic perception tasks such as object segmentation and 3D object reconstruction using a robot manipulator. Our self-supervised method can segment unknown objects from a robotic gripper in RGB video sequences by exploiting motion and temporal cues. The key aspect of our approach in contrast to existing systems is its independence of any hardware specifics such as extrinsic and intrinsic camera calibration and a robot model. We achieve this using a two-step process: First, we learn to predict segmentation masks for our given manipulator using optical flow estimation. Then, these masks are used in combination with motion cues to automatically distinguish between the manipulator, the background, and the unknown, grasped object. We perform a thorough comparison with alternative baselines and approaches in the literature. The obtained object views and masks are suitable training data for segmentation networks that generalize to novel environments and also allow for watertight 3D object reconstruction.

## I. INTRODUCTION

Despite the major advancements recently made in robotic perception, in practice there are still a lot of challenges to be solved. Two of the most prominent are (1) the lack of annotated training data for variable recognition tasks and (2) domain gaps originating from varying environments and sensors. Especially in the context of robotic manipulation accurate object segmentation is crucial. However, creating sufficient annotated object masks for training a neural network is very time consuming. For example, to label the *PASCAL VOC 2010 trainval* dataset, users spent an average of 61 seconds to draw the outlines of a single object [29].

Techniques like transfer-, semi- and meta- learning can lower the amount of necessary annotations but they do not abstain from it. Another approach is to leverage synthetic data while ensuring generalization to real data through photo-realistic rendering [58, 17], domain randomization [50, 49] or domain adaptation [53, 56]. However, creating the required 3D models is a laborious process and real labeled sensor recordings from environments relevant for execution often yield better results.

In this paper, we follow a different approach: Robots can concurrently observe and interact with objects similar to the way human infants experience objects [27, 34]. Concretely, we grasp unknown objects using a robotic manipulator, perform motions in front of a camera and analyze the differences

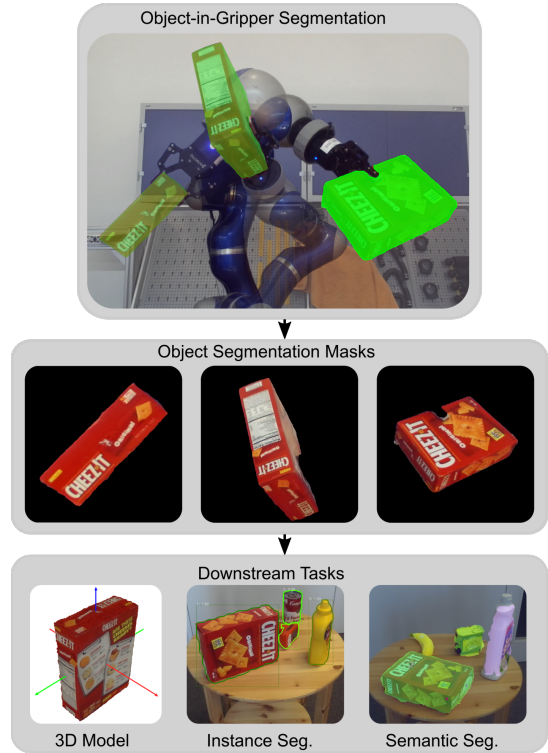


Fig. 1: Our self-supervised method is able to segment unknown objects in the gripper from robotic motions. The resulting annotation masks can be applied to several downstream tasks such as 3D modeling or as training data for instance or semantic segmentation.

over sequences of images. Thereby, we automatically obtain accurate masks of the grasped objects from any possible viewpoint. These can be used in various downstream tasks like self-supervised semantic or instance segmentation and even full 3D object reconstruction from a robotic gripper (see Figure 1).

Our method has major advantages. First, it is independent of extrinsic and intrinsic camera calibration and a robot model which makes the system robust and flexible. Second, despite minimal human intervention it leads to strong segmentation performance and outperforms competing self-supervised meth-

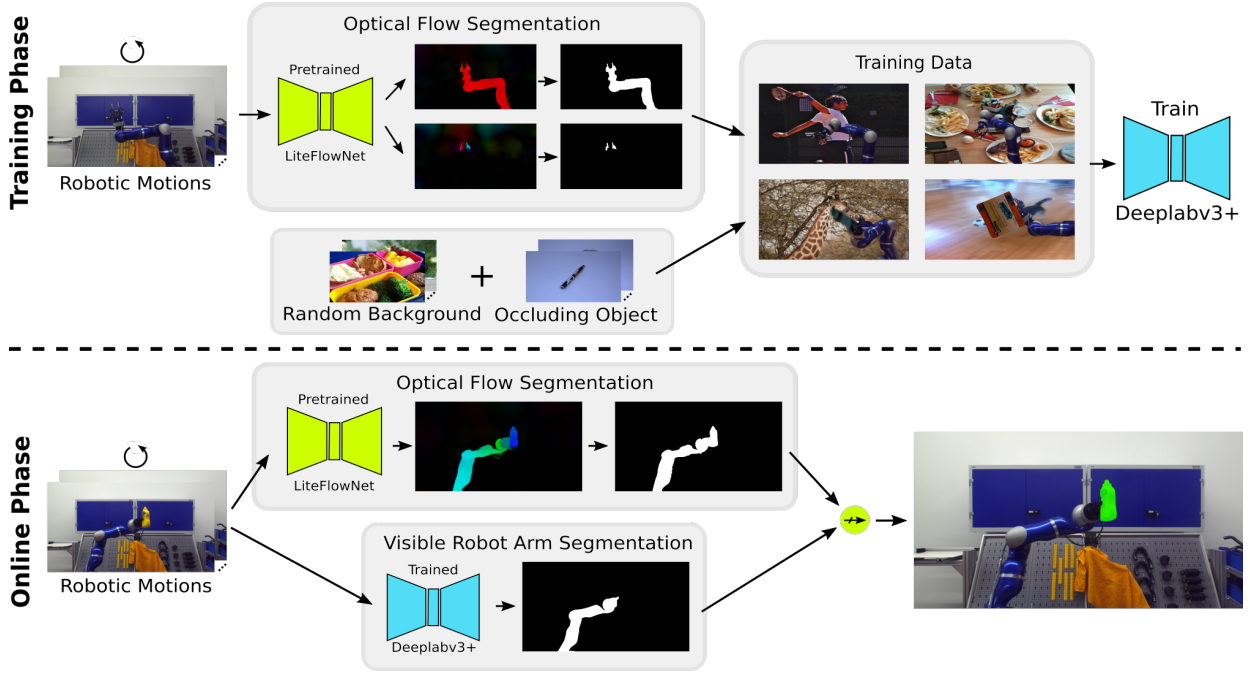


Fig. 2: In a training phase, we predict optical flow for robot arm motions using a pre-trained LiteFlowNet. By thresholding pixel-wise velocity, we generate robot masks that are used to train a Deeplabv3+ to segment the visible robot arm from randomized backgrounds. We emulate the presence of an occluding object at the gripper’s position (top). The trained CNN can then be used to separate the robot manipulator from any unknown, grasped object in the joint optical flow (bottom). The result is an abundant source of labeled data that can be produced online in any static environment.

ods. Furthermore, the data can be incrementally collected in varying test environments. Third, for the mask generation we only assume that objects are graspable and that the background is mostly static. There are no assumptions on strict object rigidity or texture.

Human vision relies on specific velocity-sensitive cells to discern objects in their field of view [31, 25]. In contrast, we rely on recent methods based on Convolutional Neural Networks (CNNs) like LiteFlowNet [19] that correlate feature maps of subsequent video frames to predict dense optical flow fields. This low-level vision task generalizes well to unseen environments and can be efficiently trained in simulation. However, optical flow alone is not sufficient to segment out the shape of the object reliably, because it can only identify the object in combination with the manipulator. And, unfortunately, current semantic segmentation networks such as DeepLabv3+ [8] or AdapNet++ [52] are not capable of segmenting out a completely unknown object (i.e. untrained class) from a robotic gripper. Therefore, we employ a two-step approach. First, we let the robot learn its own appearance by moving the manipulator in front of the camera without objects, and then train a DeepLabv3+ network to segment the shape of the manipulator from background in single frames. During inference, this trained model is used in combination with LiteFlowNet to detect the moving manipulator with the grasped object and to segment out the latter. See Figure 2 for an overview.

## II. RELATED WORK

In the context of robotics, learning from the environment by means of interacting, sensing and perceiving information is generally entitled *Interactive Perception* (IP) [6]. Of special interest are, given the context of this work, approaches that induce motion in a scene in order to perform object segmentation.

### A. Object Segmentation from Motion

Motion as additional cue is a strong enhancement for unknown object segmentation and has widely been investigated. Background subtraction entitles one of the earlier video segmentation methods and considers the alteration rate of pixels across consecutive frames. The statistical representation of a scene background can be modeled by, for instance, (multiple) Gaussian distribution(s) [57, 48] or via kernel density estimation [10]. Recently, CNNs have also been applied with promising results [22, 51, 7], albeit usually trained in a supervised manner on the problem at hand. While the mentioned approaches implement a binary segmentation, and hence can only do a fore- vs. background segmentation, our approach requires the additional distinction between robot arm and object.

In their early work, Shi and Malik [23] introduce the concept of spatio-temporal pixel clustering for object segmentation. The main idea, also applied in several other methods (e.g. [24, 15, 32]), is to group pixels based on similar motion

behavior obtained by tracking pixel motion with optical flow over a sequence. Fragkiadaki et al. [14] apply a CNN for object motion detection which is forwarded to a clustering method to obtain object masks. In [4], classical geometric knowledge via optical flow is combined hierarchically with semantic segmentation obtained by a CNN. Recently, two works propose to merge appearance (RGB) and motion (optical flow) information either in a two-stream CNN [9] or in a recurrent neural network [60]. Another learning-based approach is suggested by [44]: The proposed neural network, which is trained on synthetic data, estimates – given consecutive RGB-D frames – the object masks as well as a dense 3D motion field, also called scene flow.

### B. Robot-based object segmentation

In most cases, robots face a static scene which typically does not move by itself. A robot however can enhance visual perception by creating helpful motion in an environment, an idea which has initially been suggested by [12]. Other works follow this approach by inducing object motion via non-prehensile actions by a robot [43, 36]. In [42], generated object hypotheses are verified by pushing, and emerging feature motions are then clustered to object masks. The restriction of textured objects is then removed in the subsequent work [43] by applying color annotated stereo data for the hypotheses generation. Patten et al. [36] also use 3D data to generate a graph which represents similarity probabilities of geometric features within the scene. In the next stage, these probabilities are updated based on optical flow and geometric change detection induced by robotic manipulations. Pathak et al. [35] propose an active agent who learns to segment by trying to pick-and-place object hypotheses from one location to another. By observing eventually pixel changes within the grasp region object hypotheses are enforced.

However, merely pushing or pick-and-place objects falls short of generating diverse object views, a characteristic known to be beneficial for the generalization ability of neural networks and essential for object reconstruction. A consequential thought is to deterministically control an item’s motion in order to maximize the amount of different object views. Such task can be achieved fairly effortless by grasping the object and following a predefined trajectory, which clearly emulates the human behavior of object perception.

Most recently, Rocha et al. [38] utilize the kinematic model of a robot for the task of automatic object segmentation in a surgical setting. Given a robot-camera calibration together with a robot model, they project the latter onto the image plane. By iteratively optimizing a GrabCut [39] based cost function on a set of images followed by projecting the robot arm given the respective kinematics, they obtain segmentation labels. These are used to train a FCN, and a post-processing by a CRF results in tool segmentation. The subsequent work of [13] builds upon this and differs from the aforementioned method by using joint locations in combination with a depth sensor instead of a kinematic robot model.

The two latter approaches come close to our suggested method regarding setup and aim. Nevertheless, there are a few noteworthy differences: First, our approach neither requires a robotic model nor robot-camera calibration in any form. Second, while we use a stereo camera to record images, we solely use an RGB sequence for all tasks and do not incorporate depth imagery at all. Third, neither approach suggests optimizing the trajectory in order to maximize the object views.

## III. METHOD

In this section, we describe in detail how a combination of optical flow and learned segmentation can be leveraged to automatically segment both, a robotic arm and a grasped object from camera streams. We also present and compare against several baseline methods based on change detection and object-agnostic segmentation.

### A. Optical Flow Segmentation

*Forward optical flow* is a vector field describing the displacement directions and velocities of each pixel between two subsequent images. This underconstrained problem can be solved by means of energy-based optimization or learning-based estimation.

Real ground truth data is hardly available, but we can train CNNs on optical flow estimation in simulation. As a low-level vision task, the generalization to real data is usually robust. We use a LiteFlowNet [19] pre-trained on Chairs [11] and Things3D [30] which is able to efficiently estimate optical flow in unseen environments from a video input. By thresholding the velocity magnitude, we can then segment a moving robot arm either with or without a grasped object from static background. Similar to [55], we refrain from a predefined, hard-coded threshold which would constrain us to a specific velocity or camera resolution. Instead we apply Otsu’s binarization [33] on the flow magnitude. The algorithm searches for a threshold in a 1D histogram to separate two classes by minimizing the weighted sum of variances of these classes

$$\sigma_W^2 = \omega_0 \sigma_0^2 + \omega_1 \sigma_1^2 \quad (1)$$

where  $\sigma_{\{0,1\}}$  are the variances of two classes to be separated and  $\omega_{\{0,1\}}$  are the zeroth cumulative moments computed from the respective bins of the histogram.

Naturally, motion between two consecutive frames is of extreme importance for successful segmentation by optical flow. To alleviate this dependency you could propagate optical flow over multiple frames (e.g. [28]). However, this can lead to drift effects and propagation of erroneous regions, thus potentially worsen an initial prediction. Hence, we tackle the problem at its root by proposing a simple algorithm which creates a robot trajectory that ensures motion of the grasped object at all time, as explained in detail in Section IV-A.

Still, optical flow alone is unsuitable to distinguish a robot arm from an unknown, grasped object.

### B. Visible Robot Arm Segmentation

To accomplish this differentiation between robot arm and grasped object segmentation mask in the optical flow field we learn how to segment the robot arm from single color images. This is much simpler than predicting a segmentation mask of any grasped object directly, where visual properties (i.e., color, shape, texture) are completely unknown entities.

To automatically create diverse training data for this task, we generate robot masks by again thresholding the optical flow produced by a moving robot arm without any object in its gripper. In order to counteract under-segmentation of the LiteFlowNet we take the joint mask of forward and backward optical flow for each frame.

To prevent over-fitting on the background, we paste the extracted robot arm masks at random translation and scale on images of the MS COCO dataset [26]. This is in contrast to Florence et al. [13] who incorporate backgrounds from their test environment.

Furthermore, to emulate the presence of a grasped object, we paste one random object crop (different from our test objects) per training sample at the gripper's position. We derive these spots by opening or closing the gripper while the robot remains at a certain joint position and again measure the optical flow between the two images. Note that the occluding objects are not learned explicitly but belong to the background class. We produce 50,000 such images and train a Deeplabv3+ on semantic segmentation. Afterwards, we are able to segment the visible robot arm parts regardless of the object in the robot's gripper.

### C. Grasped Object Segmentation

At runtime, we use the same pre-trained LiteFlowNet [19] to perform optical flow segmentation (Section III-A) of the robot arm together with a grasped object. We then utilize our trained network described in the previous section to predict the segmentation mask of the visible robot. Finally, parts in motion but not detected as robot arm are denoted as the object.

### D. Change Detection

As a baseline measure we explore pixel-wise change detection [37, 46] in RGB space and between optical flow masks. Therefore, we record images of the robot arm both with and without an object at the same position by leveraging the robot's possibility of reaching the same pose in Cartesian space multiple times. Mathematically, given two images  $I_1(\mathbf{x})$  and  $I_2(\mathbf{x})$ , such a binary labeling  $B(\mathbf{x})$  can be obtained by

$$B(\mathbf{x}) = \begin{cases} 1, & \text{if } |I_1(\mathbf{x}) - I_2(\mathbf{x})| > \tau_{cd} \\ 0, & \text{otherwise.} \end{cases} \quad (2)$$

We empirically set  $\tau_{RGB} = \frac{p}{25}$  with  $p$  denoting the pixel range for the RGB case, and  $\tau_{OF} = 0$  for the binary case of optical flow masks.

Clearly, image synchronization between the two runs is of extreme importance to minimize robot pixel changes. We

achieve this by recording images while the robot stops at a particular joint configuration.

Of course, the robot arm segmentation alone could also be acquired following a sophisticated setup consisting of (1) a static camera that is accurately calibrated against the robot, (2) a full, articulated model of the robot from which we (3) render masks in corresponding joint configurations. In contrast, our method works in the camera frame only and does not assume to have prior knowledge about the robot. Thus, there are no issues with de-calibration and images can be recorded from varying camera positions.

The extracted segmentation masks of the object and the robot arm can be useful themselves in an online setting, e.g. to avoid collisions. However, our main goal is to automatically produce labels for downstream tasks like object instance segmentation from a scene.

## IV. SETUP AND DATASET CREATION

The main setup consists of a KUKA LBR4+ robot arm [1] on a linear axis with a Robotiq 2F-85 two-finger gripper [20]. Images are recorded with a ZED stereo sensor [21] under fixed exposure and white balance.

### A. Trajectory Generation

The main goal of our method is to automatically generate data for training object segmentation networks and for performing 3D object reconstruction. For both tasks it is important to obtain as diverse object views as possible. A trajectory obtained e.g. by kinesthetic teaching could instead create object views biased towards specific poses.

Even though we do not assume that the object-camera transformation is known, we can still produce nearly equally distributed end-effector rotations using Fibonacci sampling [3]. First we create an evenly distributed lattice using  $N = 301$  2D points with coordinates

$$(x_i, y_i) = \left( \frac{i + 1/2}{N}, \frac{i}{\phi} \right) \quad \text{for } 0 \leq i \leq N - 1 \quad (2)$$

where  $\phi = \frac{1+\sqrt{5}}{2}$  is the golden ratio. Then, we perform an area preserving mapping onto a cylinder and subsequently onto a sphere by

$$(x, y) \rightarrow (\theta, \phi) : \quad (\cos^{-1}(2x - 1) - \pi/2, 2\pi y) \quad (3)$$

$$(\theta, \phi) \rightarrow (x, y, z) : \quad (\cos \theta \cos \phi, \cos \theta \sin \phi, \sin \theta) \quad (4)$$

From these points on the sphere we can construct corresponding rotation matrices  $R_i$  (via up and forward vectors). However, the robot would heavily occlude the object in some of the poses where the gripper points away from the camera. Therefore, we split the view sphere in half and mirror the gripper rotations pointing away from the camera to the side that points approximately towards the camera. To obtain views from all sides, the object is rotated automatically in the gripper after the first half of rotations has been executed. An



exemplary view sphere with less points is shown in Figure 9 in the Appendix.

Additionally, some rotational end-effector movements do not create sufficient motion to reliably detect the object mask by means of optical flow. Therefore, we propose to continuously follow Cartesian points on an ellipse-shaped trajectory that is approximately parallel to the image plane. We repeatedly loop through  $n_e = 20$  equidistant points on the ellipse and use them as end-effector translations. Finally, we assign end-effector rotation matrices  $R_i$  by spiraling through the points on the sphere from the Fibonacci sampling.

### B. Robotic Arm Recordings

We use the trajectory as described in the preceding section to record images of the robot at  $N = 301$  various poses. At every configuration  $P_i$  we shift the linear axis with a small offset to ensure that all parts of the robot jointly move with the same velocity. Additionally, at every such pose we solely move the gripper to different positions to derive spots where to paste occluding objects, as explained in Section III-B.

We can realistically emulate the presence of an object if the gripper mask consists of two components. Then, we occlude the smaller one and overlay the object with the larger gripper part to synthetically emulate a grasp. Finally, we train a Deeplabv3+ on visible robot arm segmentation (training details are explained in E in the Appendix).

### C. Grasping YCB-Video Objects

To demonstrate the effectiveness of our suggested approach, we record 15 different objects of the YCB-Video Dataset [59] while being grasped by a robotic gripper. All recorded objects are depicted in Figure 8 in the Appendix.

As grasping of unknown objects is a challenging task on its own and often requires priors in the form of object poses [4, 5, 18] or the environment [41, 45], we directly put the respective object into the gripper. Nevertheless, to further automate our approach, we carry out a grasping study on these objects and present the results in Table VI in the Appendix.

### D. Post-Processing

We refine object masks to encounter false-positive and false-negative predictions of both utilized CNNs.

First, we delete all parts in contact with the image border. The object is always fully visible in the camera frame, and we hypothesize that our trained network successfully segments the area around the gripper. Hence, the object mask should be detached from all irrelevant mask fractions identified by optical flow thresholding, and every segmentation in contact with the border can be discarded. Second, we once more utilize the spots produced by opening and closing the gripper at stationary robot arm positions as estimation of the object’s position. We always keep the part of the mask that is closest to the estimated location, but reject every component that is further away than 100 pixels. Last but not least, we delete mask parts that are below 2500 pixels to remove small noisy artifacts.

## V. EVALUATION OF GRASPED OBJECT MASKS

Here, we evaluate our automatic annotation method. For all segmentation results we report the standard *mean Intersection over Union* (mIoU). Therefore, we manually annotate 15% of all recorded YCB object images with ground truth segmentation masks. The object poses of this subset are identical across all items.

### A. Comparison to Baselines

Table I reports the mIoU of two change detection baselines and our proposed method. We additionally experiment with object-agnostic segmentation, where we directly predict an object mask from a single RGB image without any knowledge of motion. Results include the post-processing steps described in Section IV-D. Additionally we list the gain in mIoU, Precision and Recall of our post-processed masks in comparison to vanilla results in Table VII in the Appendix. For equal comparison we apply the same post-processing on every method except for change detection in RGB space, where we perform simple morphological Opening and Closing.

TABLE I: Quantitative comparison of our method compared to two baseline approaches. Our approach excels in every object except for one. Numbers in **bold** denote the best results.

YCB Object	CD <sub>RGB</sub>	CD <sub>OF</sub>	Obj-Agn	Ours
003_cracker_box	34.06	70.60	57.50	<b>88.84</b>
005_tomato_soup_can	27.57	38.66	76.57	<b>81.53</b>
006_mustard_bottle	32.31	66.94	55.56	<b>86.24</b>
007_tuna_fish_can	17.87	52.69	00.00	<b>60.81</b>
008_pudding_box	46.10	64.89	76.66	<b>80.40</b>
010_potted_meat_can	34.81	71.07	75.46	<b>81.78</b>
011_banana	33.72	47.13	00.00	<b>77.23</b>
019_pitcher_base	42.05	74.66	48.87	<b>78.56</b>
021_bleach_cleanser	32.99	61.19	33.99	<b>83.82</b>
024_bowl	41.09	78.18	57.07	<b>91.19</b>
025_mug	39.38	77.26	84.73	<b>86.36</b>
035_power_drill	18.16	50.77	52.32	<b>60.69</b>
037_scissors	06.43	10.35	00.00	<b>46.01</b>
052_extra_large_clamp	38.98	52.37	00.00	<b>53.48</b>
061_foam_brick	22.10	61.69	<b>87.29</b>	80.08
Average	31.18	58.56	47.07	<b>75.80</b>

Our method outperforms the three baselines by a considerable margin across all objects except one, which is best explained in Figure 3. Clearly, change detection in RGB color space naturally fails if object and gripper share similar colors or if reflective materials are present. The algorithm suffers from sensor noise, shadows and requires a very accurate repetition of the robot trajectories with and without the object. Furthermore, deformable parts on the robot (e.g. an attached cable) cannot be distinguished from the object mask. Change detection with optical flow masks does not deal with these issues, but fails to segment object parts whenever they are located directly in front of the robot. Most notably though, both baseline methods require an additional recording of images without the object in gripper, which has to be done for every object individually due to the different gripper positions during the grasp. Altogether, the resulting constraints are impractical in real world robotic applications.

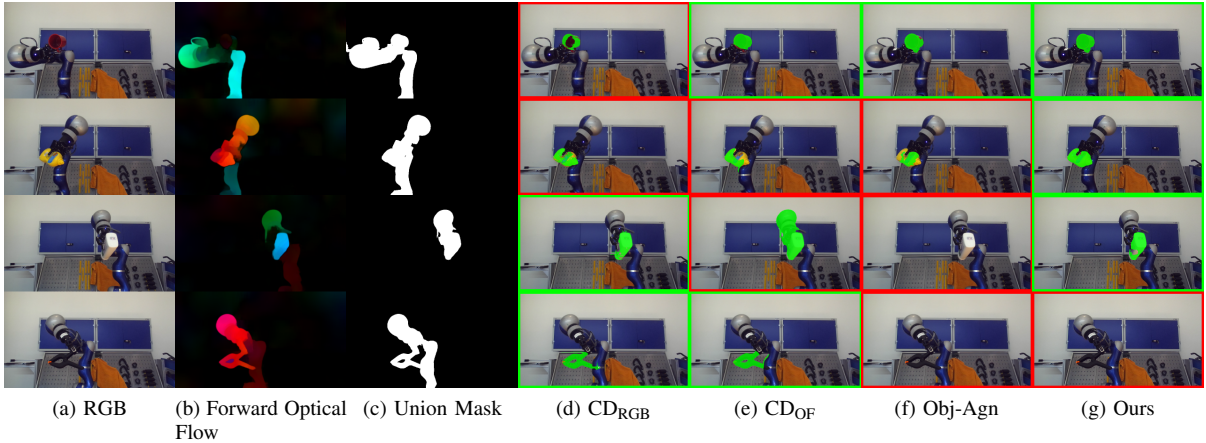


Fig. 3: Exemplary qualitative results of our method and the three baselines (best viewed in color). Red borders denote poor performance, while green ones indicate satisfactory segmentation masks. Top row:  $CD_{RGB}$  tends to perform poorly whenever object and background are of similar color. Note that while  $CD_{OF}$  and Obj-Agn deliver decent result despite small cut-off parts, our method even successfully segments the handle (best viewed zoomed-in). Second row:  $CD_{OF}$  can only segment moving parts as object which are directly located in front of the background. Third row:  $CD_{OF}$  oversegmentation due to faulty LiteFlowNet prediction, which our method corrects. Fourth row: An extreme failure case of our method where parts of the object are identified as robot due to the similar color and texture of clamp and gripper. Our applied post-processing delete the remaining small blobs and lead to an empty mask. Obj-Agn fails to segment the last two objects completely.

Our proposed pipeline is insensitive against these issues, since the optical flow and robot segmentation networks are trained to extract features that are robust against noise, lighting changes, similar colors and non-rigid parts. After training the segmentation network, trajectories with a grasped object alone contain all necessary information to extract object masks. We also circumvent the tough task of learning how to segment unknown objects which can be ill-defined. Our object-agnostic comparison underlines this as some items are not identified at all - unlike to our approach, where an object is simply defined as a physically connected thing in motion.

We still identify difficulties for small, thin objects like the *scissors* or objects that share texture and color of the gripper (the *clamp*) in our current approach, and the respective metrics are the lowest across all objects.

### B. Comparison to Literature

To the best of our knowledge, the most similar approach in literature stems from Florence et al. [13]. Yet, they require robot-camera calibration as well as depth information and obtain their foreground mask with Grabcut [39], while the distinction between robot and object is done in a similar fashion with a CNN. We compare our method on a joint subset of YCB objects. Results can be found in Table II.

Although we refrain from a robot model, calibration and solely utilize a single RGB image stream, we are able to surpass their respective baseline. However, we under-perform notably for the *pitcher*, an item that is of similar color as both robot arm and background, and the *scissors*, mainly due to its thin shape which often gets misclassified by the LiteFlowNet.

TABLE II: Comparison to Florence et al. [13] whom we outperform by 2.3 percent points, especially due to the superior performance on the *banana* and *foam brick* of our method. Numbers in **bold** denote the best results.

YCB Object	[13]	Ours
011_banana	54.60	<b>77.23</b>
019_pitcher_base	<b>91.90</b>	78.56
024_bowl	90.10	<b>91.19</b>
025_mug	84.30	<b>86.36</b>
035_power_drill	<b>62.60</b>	60.69
037_scissors	<b>62.70</b>	46.01
061_foam_brick	57.40	<b>80.08</b>
Average	71.94	<b>74.30</b>

Sauer et al. [40] propose a framework for object tracking which automatically selects additional templates based on the diversity to existing ones. It can be used on top of already existing siamese feature extractors, and we further investigate the performance of our masks with a pre-trained SiamMask tracker [54] which is capable of segmenting the object of interest at the same time. Initial bounding boxes are derived from a randomly picked mask. We also experiment with providing additional masks to initialize the tracker's templates. We use both ground truth annotations as well as our predictions to simultaneously observe the performance of our proposed method in another context. Results averaged across five runs are depicted in Table III and clearly indicate that THOR is not applicable for deriving masked object views with a robotic arm. While the algorithm works well in distinct cases (identifiable through the high  $STD_{objects}$ ), it fails to

successfully track small objects or ones that have similar color to surrounding parts. Often, the tracker attaches to the latter and loses the object.

TABLE III: Differences between ground truth masks and our predicted masks for segmentation with THOR [40].  $STD_{runs}$  refers to the standard deviation across five runs with different randomly picked masks as initialization, while  $STD_{objects}$  denotes the standard deviation across objects. *Predicted* refers to the predictions with mIoU as in Table I

Setting	mIoU	$STD_{runs}$	$STD_{objects}$
Ground Truth Bounding Boxes	29.20	$\pm 01.17$	$\pm 21.85$
+ 4 templates	29.62	$\pm 02.13$	$\pm 19.87$
+ 14 templates	30.64	$\pm 02.08$	$\pm 22.24$
Predicted Bounding Boxes	24.65	$\pm 03.75$	$\pm 16.02$
+ 4 templates	30.14	$\pm 04.13$	$\pm 20.32$
+ 14 templates	29.87	$\pm 01.73$	$\pm 20.36$
Ours	75.80		

### C. Ablation Study

In the following Table IV we investigate the influence of different design choices for our method regarding data generation / training setting and post-processing.

TABLE IV: Ablation study on different data augmentation and training settings (*D/T*) and post-processing (*PP*) across different flow masks (from which we subtract the robot prediction to derive an object mask). In every consecutive row we drop the respective step and all previous ones. Altogether we are able to boost object-in-gripper segmentation from an initial object mIoU of around 51% by about 25 percent points.

		Forward Flow	Intersection	Union
	Ours	<b>76.32</b>	72.15	75.80
PP	- Min. mask size	65.54	57.29	<b>68.04</b>
	- Max. grip. dist.	60.01	53.63	<b>61.50</b>
	- Border deletion	57.61	53.47	<b>58.29</b>
D/T	- Gripper loss weight	56.24	51.22	<b>57.55</b>
	- Occluding object	<b>51.79</b>	48.14	51.70

The main success factors for our final metrics are the pasting of an distractor object, the maximum gripper distance and the minimum mask size. Flow intersection masks, on the other hand, might eliminate noise but heavily rely on motion at the same spatial positions between consecutive frames. Even with perfect continuous movement this can not be guaranteed due to potential mis-predictions of the LiteFlowNet.

### D. Object Segmentation from Scenes

In the following, we use the generated object masks to train Deeplabv3+ on semantic segmentation from RGB scenes (for training settings please see Section E in the Appendix). We test our model on 100 images where we place the respective objects at random position and orientation on a table, as shown in Figure 5. Quantitative results for semantic segmentation can be found in Table V. Even though the test set was

TABLE V: Quantitative results of object segmentation from scenes. Average mIoU, Precision and Recall are, respectively, 86.49%, 91.71% and 93.95% of the initial object-in-gripper segmentation. All values are in %.

YCB Object	mIoU	Precision	Recall
003_cracker_box	74.29	79.93	91.32
005_tomato_soup_can	62.49	65.32	93.53
006_mustard_bottle	79.77	95.90	82.58
007_tuna_fish_can	51.27	56.21	85.36
008_pudding_box	73.78	78.73	92.15
010_potted_meat_can	63.87	74.25	82.05
011_banana	75.18	82.52	86.14
019_pitcher_base	88.75	92.74	95.37
021_bleach_cleanser	54.01	55.51	95.23
024_bowl	53.69	55.02	95.67
025_mug	52.68	84.61	58.27
035_power_drill	77.72	81.67	94.13
037_scissors	42.35	49.14	75.39
052_extra_large_clamp	58.68	86.23	64.75
061_foam_brick	74.83	86.43	84.78
Average	65.56	75.15	85.12

recorded in a different environment than the training data, the objects *pitcher* and *drill* receive higher mIoU scores (Table V) than when segmented in the gripper (Table I). The high recall across almost all objects further suggests the applicability of semantic segmentation with our automatically generated masks. However, although the *mug* and *bowl* stood out during the automatic mask generation, the network seems to have difficulties differentiating between them since they have very similar texture. We hypothesize that this is because of incomplete masks which provide insufficient information on the object's shape.

We also train MaskRCNN [16] on instance segmentation using the same training data and qualitatively compare results to a MaskRCNN trained on the YCB Video dataset in Figure 6. It shows that our grasped object data generalizes to novel settings while training on YCB Video does not generalize to a novel sensor. Contrary to the findings above, the mug gets identified very well (first row, second image). This can be explained by the fact that the MaskRCNN first crops the image into regions of interest and then segments these - an arguably simpler task as opposed to direct full-image semantic segmentation.

Convolutional Neural Networks typically require many different views of an object to derive a good understanding of the item and generalize well onto unknown scenes. With our initial  $n = 301$  almost equidistant views on a sphere onto an object we investigate the performance loss onto the same test scene given less views. Interestingly, merely two views of an object provide sufficient information to achieve 60% of the mIoU with 301 views, as shown in Figure 4.

### E. Photogrammetric 3D Object Reconstruction

Textured 3D meshes contain rich information about objects. In robotics they can be utilized for grasp planning, object pose estimation or tracking and learning in simulation. A robot

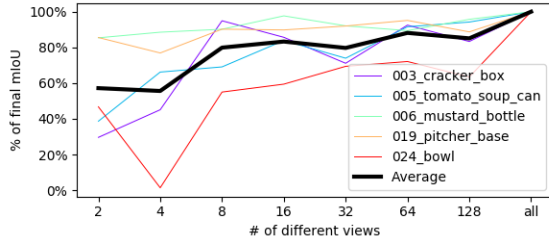


Fig. 4: Number of different views in relation to the relative final mIoU with all object views for five different objects. With only two viewpoints the network achieves on average 60% of the final mIoU (301 poses).



Fig. 5: Cropped views of our test scene with colorized semantic segmentation predictions. The objects in the left two pictures get segmented well while there are failure cases on the right.

that can perform 3D object reconstruction without human intervention therefore strongly increases autonomy.

Photogrammetric 3D object reconstruction is usually performed by taking photos of a static object from various camera positions, finding correspondences, computing their 3D coordinates and thereof building a mesh. Disadvantages of this method are that the bottom of the object is usually not captured and that the environment and object should be static at all times. Since our presented methods yield accurate segmentation masks, we can reverse the problem by actively record views of a rotating object using a static camera. One challenge is that the lighting on the object is dynamic during the recording process. Nonetheless, our masked object views can be successfully fused without manual intervention or tuning using the reconstruction software Agisoft Metashape [2]. Figure 7 shows the resulting textured mesh of the YCB Cracker Box and the euclidean distances of the nearest vertices on the aligned ground truth model. Please note that pure monocular photogrammetric 3D object reconstruction can also fail for some symmetric and texture-less objects. In these cases, information from depth cameras should be incorporated.

## VI. CONCLUSION

We have presented methods to automatically generate unseen object and robot arm segmentation masks through robotic interactions. Our optical flow based approach assumes low prior knowledge and few assumptions on the setup. Particularly, the camera does not need to be calibrated against the robot and can thus be arbitrarily moved. A wide range

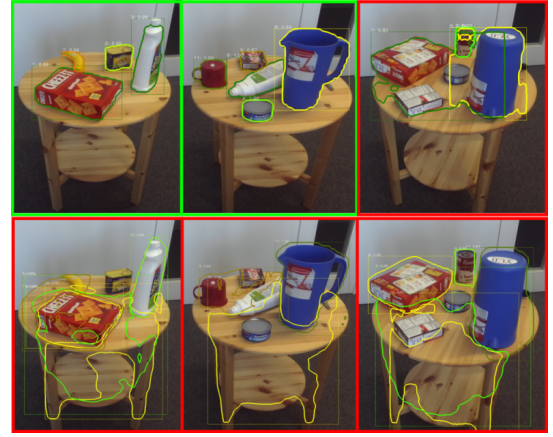


Fig. 6: Top row: MaskRCNN trained on the grasped objects; Bottom row: MaskRCNN trained on the YCB Video dataset [59]; Note that the data from grasped objects generalizes to table top scenes while the domain gap to the YCB Video dataset that consists of table top scenes but uses a different sensor is too large.

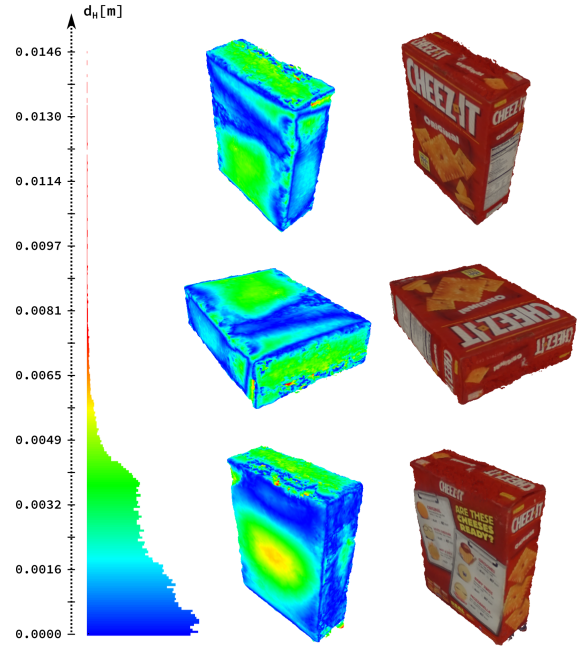


Fig. 7: Photogrammetric 3D Reconstruction of YCB Cracker Box directly from the robotic gripper; Left: Histogram of euclidean distances  $d_H$  from nearest vertices between ground truth mesh (YCB Video dataset [59]) and our aligned 3D reconstruction. The mean distance between vertices is  $\mu(d) = 0.2cm$ ; Middle: Quality Mapping; Right: Texture Mapping; Note that the gripper was successfully removed from the object.

of graspable, potentially non-rigid, objects can be processed while having few restrictions on the choice of the robot arm



and gripper. The usability of the generated labels has been demonstrated in several downstream tasks like semantic and instance segmentation from scenes and 3D object reconstruction. The latter is a step forward to close the sim2real cycle.

Our work has been motivated by both, the way humans learn through object interactions and practical limitations of supervised learning algorithms stemming from the lack of annotated data. We conclude that observing self-generated motions can enable robots to semi-autonomously learn about newly encountered objects which is a prerequisite for self-improving systems.

#### REFERENCES

- [1] KUKA AG. LBR iiwa. *KUKA AG, Augsburg, Germany*, accessed November, 2019.
- [2] LLC Agisoft. Agisoft metashape user manual, Professional edition, Version 1.5. *Agisoft LLC, St. Petersburg, Russia*, accessed June, 2018.
- [3] Álvaro González. Measurement of Areas on a Sphere Using Fibonacci and Latitude–Longitude Lattices. *Mathematical Geosciences*, 42(1):49–64, Nov 2009.
- [4] Pia Bideau, Aruni RoyChowdhury, Rakesh R. Menon, and Erik Learned-Miller. The Best of Both Worlds: Combining CNNs and Geometric Constraints for Hierarchical Motion Segmentation. In *The IEEE Conference on Computer Vision and Pattern Recognition (CVPR)*, June 2018.
- [5] Jeannette Bohg and Danica Kragic. Learning Grasping Points with Shape Context. *Robot. Auton. Syst.*, 58(4): 362–377, April 2010.
- [6] Jeannette Bohg, Karol Hausman, Bharath Sankaran, Oliver Brock, Danica Kragic, Stefan Schaal, and Gaurav S. Sukhatme. Interactive Perception: Leveraging Action in Perception and Perception in Action. *IEEE Transactions on Robotics*, (6):1273–1291, Dec 2017.
- [7] Thierry Bouwmans, Sajid Javed, Maryam Sultana, and Soon Ki Jung. Deep Neural Network Concepts for Background Subtraction: A Systematic Review and Comparative Evaluation. *Neural Networks*, 117:8–66, 2019.
- [8] Liang-Chieh Chen, Yukun Zhu, George Papandreou, Florian Schroff, and Hartwig Adam. Encoder-Decoder with Atrous Separable Convolution for Semantic Image Segmentation, 2018.
- [9] Achal Dave, Pavel Tokmakov, and Deva Ramanan. Towards Segmenting Everything That Moves. *CoRR*, abs/1902.03715, 2019.
- [10] Achmed Elgammal, Ramani Duraiswami, David Harwood, and Larry S. Davis. Background and foreground modeling using nonparametric kernel density estimation for visual surveillance. *Proceedings of the IEEE*, 90(7): 1151–1163, July 2002.
- [11] Philipp Fischer, Alexey Dosovitskiy, Eddy Ilg, Philip Häusser, Caner Hazirbas, Vladimir Golkov, Patrick van der Smagt, Daniel Cremers, and Thomas Brox. FlowNet: Learning Optical Flow with Convolutional Networks. *CoRR*, abs/1504.06852, 2015.
- [12] Paul Fitzpatrick and Giorgio Metta. Grounding vision through experimental manipulation. *Philosophical Transactions of the Royal Society of London. Series A: Mathematical, Physical and Engineering Sciences*, 361 (1811):2165–2185, August 2003.
- [13] Victoria Florence, Jason J. Corso, and Brent Griffin. Self-Supervised Robot In-hand Object Learning. *CoRR*, abs/1904.00952, 2019.
- [14] Katerina Fragkiadaki, Pablo Arbelaez, Panna Felsen, and Jitendra Malik. Learning to segment moving objects in videos. In *Proc. IEEE Conf. on Computer Vision and Pattern Recognition (CVPR)*, pages 4083–4090, 2015.
- [15] Matthias Grundmann, Vivek Kwatra, Mei Han, and Irfan Essa. Efficient Hierarchical Graph Based Video Segmentation. *Proc. IEEE Conf. on Computer Vision and Pattern Recognition (CVPR)*, 2010.
- [16] Kaiming He, Georgia Gkioxari, Piotr Dollár, and Ross Girshick. Mask R-CNN. *arXiv preprint arXiv:1703.06870*, 2017.
- [17] Tomas Hodan, Vibhav Vineet, Ran Gal, Emanuel Shalev, Jon Hanzelka, Treb Connell, Pedro Urbina, Sudipta N Sinha, and Brian Guenter. Photorealistic Image Synthesis for Object Instance Detection. *arXiv preprint arXiv:1902.03334*, 2019.
- [18] Kaijen Hsiao, Sachin Chitta, Matei Ciocarlie, and E. Gil Jones. Contact-reactive grasping of objects with partial shape information. In *2010 IEEE/RSJ International Conference on Intelligent Robots and Systems*, pages 1228–1235, Oct 2010.
- [19] Tak-Wai Hui, Xiaoou Tang, and Chen Change Loy. Lite-FlowNet: A Lightweight Convolutional Neural Network for Optical Flow Estimation. In *Proc. IEEE Conf. on Computer Vision and Pattern Recognition (CVPR)*, pages 8981–8989, June 2018.
- [20] Robotiq Inc. 2F-85 and 2F-140 Grippers. *Robotiq Inc., Quebec, Canada*, accessed August, 2019.
- [21] Streolabs Inc. ZED. <https://www.stereolabs.com/zed/>, 2020. Accessed: 2020-01-22.
- [22] Suyog Dutt Jain, Bo Xiong, and Kristen Grauman. FusionSeg: Learning to combine motion and appearance for fully automatic segmentation of generic objects in videos. *CoRR*, abs/1701.05384, 2017.
- [23] Jianbo Shi and Jitendra Malik. Motion segmentation and tracking using normalized cuts. In *IEEE International Conference on Computer Vision (ICCV)*, pages 1154–1160, Jan 1998.
- [24] Margret Keuper, Bjoern Andres, and Thomas Brox. Motion Trajectory Segmentation via Minimum Cost Multicuts. In *IEEE International Conference on Computer Vision (ICCV)*, pages 3271–3279, Dec 2015.
- [25] Denis N Lee. The optic flow field: The foundation of vision. *Philosophical Transactions of the Royal Society of London. B, Biological Sciences*, 290(1038):169–179, 1980.
- [26] Tsung-Yi Lin, Michael Maire, Serge J. Belongie, Lubomir D. Bourdev, Ross B. Girshick, James Hays,



- Pietro Perona, Deva Ramanan, Piotr Dollár, and C. Lawrence Zitnick. Microsoft COCO: Common Objects in Context. *CoRR*, abs/1405.0312, 2014.
- [27] Michele A. Lobo, Elena Kokkoni, Ana Carolina de Campos, and James C. Galloway. Not just playing around: infants’ behaviors with objects reflect ability, constraints, and object properties. *Infant Behav Dev*, 37(3):334–351, Aug 2014.
- [28] Tan Khoa Mai, Michèle Gouiffès, and Samia Bouchafa. Optical Flow Refinement using Reliable Flow Propagation. In *VISIGRAPP*, 2017.
- [29] Subhransu Maji. Large Scale Image Annotations on Amazon Mechanical Turk. Technical Report UCB/EECS-2011-79, EECS Department, University of California, Berkeley, Jul 2011.
- [30] Nikolaus Mayer, Eddy Ilg, Philip Häusser, Philipp Fischer, Daniel Cremers, Alexey Dosovitskiy, and Thomas Brox. A Large Dataset to Train Convolutional Networks for Disparity, Optical Flow, and Scene Flow Estimation. *CoRR*, abs/1512.02134, 2015.
- [31] K. Nakayama and J. M. Loomis. Optical Velocity Patterns, Velocity-Sensitive Neurons, and Space Perception: A Hypothesis. *Perception*, 3(1):63–80, 1974. PMID: 4444922.
- [32] Peter Ochs, Jitendra Malik, and Thomas Brox. Segmentation of Moving Objects by Long Term Video Analysis. 36(6):1187–1200, June 2014.
- [33] N. Otsu. A Threshold Selection Method from Gray-Level Histograms. *IEEE Transactions on Systems, Man, and Cybernetics*, 9(1):62–66, Jan 1979.
- [34] Scott P Johnson. How Infants Learn About the Visual World. *Cognitive science*, 34:1158–1184, 09 2010.
- [35] Deepak Pathak, Yide Shentu, Dian Chen, Pulkit Agrawal, Trevor Darrell, Sergey Levine, and Jitendra Malik. Learning Instance Segmentation by Interaction. 2018.
- [36] Timothy Patten, Michael Zillich, and Markus Vincze. Action Selection for Interactive Object Segmentation in Clutter. In *2018 IEEE/RSJ International Conference on Intelligent Robots and Systems (IROS)*, pages 6297–6304, Oct 2018.
- [37] Richard Radke, Srinivas Andra, Omar Al-Kofahi, and Badrinath Roysam. Image change detection algorithms: A systematic survey. 14:294–307, 04 2005.
- [38] Cristian Rocha, Nicolas Padoy, and Benoit Rosa. Self-Supervised Surgical Tool Segmentation using Kinematic Information, 02 2019.
- [39] Carsten Rother, Vladimir Kolmogorov, and Andrew Blake. GrabCut - Interactive Foreground Extraction using Iterated Graph Cuts. *ACM Transactions on Graphics (SIGGRAPH)*, August 2004.
- [40] Axel Sauer, Elie Aljalbout, and Sami Haddadin. Tracking Holistic Object Representations, 2019.
- [41] Ashutosh Saxena, Justin Driemeyer, and Andrew Y. Ng. Robotic Grasping of Novel Objects using Vision. *The International Journal of Robotics Research*, 27(2):157–173, 2008.
- [42] David Schiebener, Aleš Ude, Jun Morimoto, Tamin Asfour, and Rüdiger Dillmann. Segmentation and learning of unknown objects through physical interaction. In *2011 11th IEEE-RAS International Conference on Humanoid Robots*, pages 500–506, Oct 2011.
- [43] David Schiebener, Aleš Ude, and Tamin Asfour. Physical interaction for segmentation of unknown textured and non-textured rigid objects. In *2014 IEEE International Conference on Robotics and Automation (ICRA)*, pages 4959–4966, May 2014.
- [44] Lin Shao, Parth Shah, Vikranth Dwaracherla, and Jeanette Bohg. Motion-based Object Segmentation based on Dense RGB-D Scene Flow. *CoRR*, abs/1804.05195, 2018.
- [45] Jane Shi and Gurdarshan S. Koonjul. Real-time Grasp Planning with Environment Constraints. 09 2014.
- [46] Ashbindu Singh. Review Article Digital change detection techniques using remotely-sensed data. *International Journal of Remote Sensing*, 10(6):989–1003, 1989.
- [47] sniklaus. pytorch-liteflownet, 2019.
- [48] Chris Stauffer and W. Eric L. Grimson. Learning patterns of activity using real-time tracking. *IEEE Transactions on Pattern Analysis and Machine Intelligence*, 22(8):747–757, Aug 2000.
- [49] Martin Sundermeyer, Zoltan-Csaba Marton, Maximilian Durner, Manuel Brucker, and Rudolph Triebel. Implicit 3d orientation learning for 6d object detection from rgb images. In *Proceedings of the European Conference on Computer Vision (ECCV)*, pages 699–715, 2018.
- [50] Josh Tobin, Rachel Fong, Alex Ray, Jonas Schneider, Wojciech Zaremba, and Pieter Abbeel. Domain randomization for transferring deep neural networks from simulation to the real world. In *2017 IEEE/RSJ international conference on intelligent robots and systems (IROS)*, pages 23–30. IEEE, 2017.
- [51] Pavel Tokmakov, Cordelia Schmid, and Karteek Alahari. Learning to segment moving objects. *International Journal of Computer Vision*, 127(3):282–301, 2019.
- [52] Abhinav Valada, Rohit Mohan, and Wolfram Burgard. Self-supervised model adaptation for multimodal semantic segmentation. *arXiv preprint arXiv:1808.03833*, 2018.
- [53] Mei Wang and Weihong Deng. Deep Visual Domain Adaptation: A Survey. *CoRR*, abs/1802.03601, 2018.
- [54] Qiang Wang, Li Zhang, Luca Bertinetto, Weiming Hu, and Philip H. S. Torr. Fast Online Object Tracking and Segmentation: A Unifying Approach, 2018.
- [55] Shui-gen Wei, Lei Yang, Zhen Chen, and Zhen feng Liu. Motion Detection Based on Optical Flow and Self-adaptive Threshold Segmentation. *Procedia Engineering*, 15:3471–3476, 2011. CEIS 2011.
- [56] Garrett Wilson and Diane J. Cook. Adversarial Transfer Learning. *CoRR*, abs/1812.02849, 2018.
- [57] C.R. Wren, A. Azarbayejani, T. Darrell, and A.P. Pentland. Pfunder: real-time tracking of the human body. *IEEE Transactions on Pattern Analysis and Machine Intelligence*, 19(7):780–785, July 1997.

- [58] Magnus Wrenninge and Jonas Unger. Synscapes: A Photorealistic Synthetic Dataset for Street Scene Parsing. *CoRR*, abs/1810.08705, 2018.
- [59] Yu Xiang, Tanner Schmidt, Venkatraman Narayanan, and Dieter Fox. PoseCNN: A Convolutional Neural Network for 6D Object Pose Estimation in Cluttered Scenes. *CoRR*, abs/1711.00199, 2017.
- [60] Christopher Xie, Yu Xiang, Dieter Fox, and Zaïd Harchaoui. Object Discovery in Videos as Foreground Motion Clustering. *CoRR*, abs/1812.02772, 2018.

## APPENDIX

### A. Grasping

To further automate our segmentation pipeline we evaluate grasping and re-grasping after placing success on the YCB objects in Table VI. The re-grasping at  $180^\circ$  degree gripper rotation is necessary as we want to record the backside of the object. Here, solely the object’s position on the table is known to the robot. Only the *bowl* cannot be grasped at a static position from top-down. The *scissors* is unstable and slightly offset when placed back onto the table so that the re-grasp at  $180^\circ$  gripper rotation can fail. Apart from these issues, the results confirm that our strategy is successful for almost all objects and depicts a practical way to minimize human intervention.

TABLE VI: Top-Down grasp successes for YCB objects. *Re-graspable* refers to placing the object and re-grasping it at  $180^\circ$  rotated gripper position.

YCB Object	graspable	re-graspable
003_cracker_box	✓	✓
005_tomato_soup_can	✓	✓
006_mustard_bottle	✓	✓
007_tuna_fish_can	✓	✓
008_pudding_box	✓	✓
010_potted_meat_can	✓	✓
011_banana	✓	✓
019_pitcher_base	✓	✓
021_bleach_cleanser	✓	✓
024_bowl	✗	✗
025_cup	✓	✓
035_power_drill	✓	✓
037_scissors	✓	✗
052_extra_large_clamp	✓	✓
061_foam_brick	✓	✓
Total	14/15	13/15

### B. YCB Objects used in this work

Figure 8 shows all 15 YCB Video objects used in this work.



Fig. 8: The 15 items from the YCB Video Objects which are used in our experiments.

### C. Fibonacci visualization

A visualization of almost equidistant points on a sphere is depicted in Figure 9.

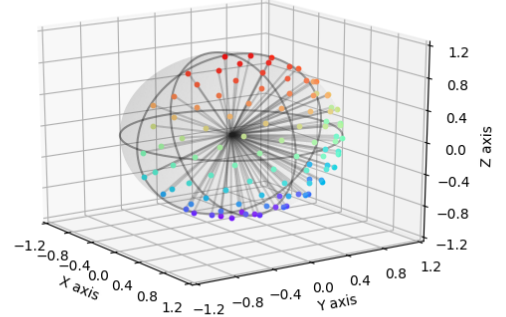


Fig. 9: Visualization of Fibonacci sampling [3] of almost equidistant points on a sphere. We only consider the end-effector rotations pointing approximately towards the camera and then regrasp the object for the back side of the sphere.

### D. mIoU, Precision and Recall between Vanilla and Post-Processed Results

Table VII lists the gain in % for different metrics for three baselines and our proposed approach.

TABLE VII: Quantitative comparison between vanilla results and applied post-processing. The metrics denote the respective average across all object classes. Especially noteworthy are the small differences between our vanilla and  $CD_{OF}$  post-processed results. All values are in %. Numbers in **bold** denote the best results.

Method	Vanilla			With Post-Processing		
	mIoU	Precision	Recall	mIoU	Precision	Recall
$CD_{RGB}$	10.88	11.57	72.66	31.18	60.19	39.31
$CD_{OF}$	38.71	44.87	73.84	58.56	69.53	78.35
Obj-Agn	34.36	<b>72.22</b>	38.24	47.07	66.94	50.27
Ours	<b>58.29</b>	63.79	<b>85.42</b>	<b>75.80</b>	<b>81.94</b>	<b>90.60</b>

### E. Training Details

Regarding the visible robot arm segmentation, our validation set consists of novel robot poses as well as unseen occluding objects, and we take the model which performs best on this split. We apply random color jitter on the occluding objects with focus on blueish augmentation to account for over-segmentation on our blue-biased robot arm. To ensure that the model is able to differentiate well between gripper and object, we weight the area around the gripper with a Gaussian shape when calculating the loss. The respective center is again

obtained from the gripper spots. We empirically set the width to 50 pixels and the magnitude at the center to a factor of 3.

We use a Deeplabv3+ implementation in PyTorch pre-trained on ImageNet. For all object-in-gripper segmentation tasks we use the default learning rate with a polynomial decay and Adam optimizer. We train with a fixed input size of 414x736 pixels.

For all optical flow predictions we use a LiteFlowNet implementation [47] pre-trained on Things3D and Chairs. We predict with a fixed input size of 414x736 pixels.

For the semantic segmentation we use the same Deeplabv3+ but freeze the encoder. The decoder is trained with a reduced learning rate of 0.0007. Similar to the robot arm segmentation, we paste multiple instances on COCO Backgrounds at random scale, translation and in-plane rotation and adapt the labels accordingly. We allow occlusions up to 60% of each object instance mask and re-sample the training image if this limit is exceeded. Thereby, we produce 50,000 images. As the objects differ in size, we weight the object classes inversely proportional by the number of pixels to put equal focus on smaller objects, and clip the background weight to the factor of the largest object class.

We train the MaskRCNN with the standard settings and refer the reader to [16] for further details.